

# First disk-resolved spectroscopy of (4) Vesta<sup>☆</sup>

Benoît Carry<sup>a,b</sup>, Pierre Vernazza<sup>c</sup>, Christophe Dumas<sup>b</sup>, Marcello Fulchignoni<sup>a</sup>

<sup>a</sup>LESIA, Observatoire de Paris-Meudon, 5 place Jules Janssens, 92195 Meudon Cedex, France

<sup>b</sup>ESO, Alonso de Córdova 3107, Vitacura, Casilla 19001, Santiago de Chile, Chile

<sup>c</sup>Research and Scientific Support Department, European Space Agency, Keplerlaan 1, 2201 AZ Noordwijk, The Netherlands

---

## Abstract

Vesta, the second largest Main Belt asteroid, will be the first to be explored in 2011 by NASA's Dawn mission. It is a dry, likely differentiated body with spectrum suggesting that it has been resurfaced by basaltic lava flows, not too different from the lunar maria.

Here we present the first disk-resolved spectroscopic observations of an asteroid from the ground. We observed (4) Vesta with the ESO-VLT adaptive optics equipped integral-field near-infrared spectrograph SINFONI, as part of its science verification campaign. The highest spatial resolution of  $\sim 90$  km on Vesta's surface was obtained during excellent seeing conditions ( $0.5''$ ) in October 2004.

We observe spectral variations across Vesta's surface that can be interpreted as variations of either the pyroxene composition, or the effect of surface aging. We compare Vesta's 2 micron absorption band to that of howardite-eucrite-diogenite (HED) meteorites that are thought to originate from Vesta, and establish particular links between specific regions and HED subclasses. The overall composition is found to be mostly compatible with howardite meteorites, although a small area around  $180^\circ$  East longitude could be attributed to a diogenite-rich spot. We finally focus our spectral analysis on the characteristics of Vesta's bright and dark regions as seen from Hubble Space Telescope's visible and Keck-II's near-infrared images.

**Key words:** ASTEROID VESTA, ASTEROIDS, SURFACES, ADAPTIVE OPTICS, INFRARED OBSERVATIONS

---

## 1. Introduction

Vesta, with a mean radius of  $265 \pm 5$  km [Thomas et al., 1997a,b], is the second largest Main Belt asteroid. It orbits the Sun at a semi-major axis of  $a = 2.36$  AU. It is the only known differentiated asteroid with an intact internal structure, presumably consisting of a metal core, an ultramafic mantle, and a basaltic crust [see Keil, 2002, for a review]. The igneous nature of its surface material was diagnosed in the early seventies [McCord et al., 1970] and subsequently confirmed by additional observations [Larson and Fink, 1975; McFadden et al., 1977; Binzel et al., 1997; Gaffey, 1997; Vernazza et al., 2005]. Two decades ago, Vesta was still the only known asteroid with a basaltic surface until Binzel and Xu [1993] discovered several main-belt asteroids with diameters  $< 10$  km and surface composition similar to Vesta's [see Pieters et al., 2006, for a review]. Those V-type asteroids were identified as members of Vesta's dynamical family [the so-called Vestoids: Williams, 1989; Zappala et al., 1990; Marzari et al., 1996]. The hypothesis of a large collision on Vesta [Marzari et al., 1996] has been confirmed by Hubble Space Telescope (HST) observations revealing the presence of a  $\sim 460$  km basin on its surface [ $1.7\times$  Vesta's radius, Thomas et al., 1997a], which is most likely the result of an impact with a  $\sim 35$  km projectile [Asphaug, 1997]. Several other V-type asteroids have seen

been discovered among the Near-Earth Asteroids (NEA) population [Xu et al., 1995; Binzel et al., 2004; Marchi et al., 2005b], and main-belt (1459 Magnya with a semi-major axis of 3.14 AU [Lazzaro et al., 2000] and some others in the middle belt [Moskovitz et al., 2008]).

Spectroscopic observations at visible [McCord et al., 1970] and near-infrared (NIR) [Larson and Fink, 1975; Feierberg et al., 1980; Feierberg and Drake, 1980] wavelengths revealed that the disk-integrated spectrum of Vesta displays strong similarities with laboratory spectra of howardite, eucrite and diogenite (HED) meteorites, McCord et al. [1970] implying quite naturally that HED meteorites came from Vesta. Later, Earth-based [Gaffey, 1997; Vernazza et al., 2005] rotationally resolved disk-integrated spectrophotometric measurements confirmed a geologically heterogeneous surface [e.g. Gaffey, 1983], consistent with the composition of HED meteorites [see the review by Keil, 2002].

Multiband disk-resolved imaging at four different visible wavelengths (0.439, 0.673, 0.953 and  $1.042 \mu\text{m}$ ) with HST [Zellner et al., 1997] have revealed various high contrast albedo marks across its surface [Binzel et al., 1997], also observed by Keck in the near-IR [ $2$  and  $3.6 \mu\text{m}$ , Zellner et al., 2005].

Several scenarios have been proposed to explain these strong albedo variations. Binzel et al. [1997] suggested differences in mineralogy, grain size, or space weathering processes. Zellner et al. [2005] discussed that Vesta's dark regions may be "impact basins" later filled with basaltic lavas, much like the lunar maria. Interestingly, Thomas et al. [1997a] found a correla-

---

<sup>☆</sup>Based on observations collected at the European Southern Observatory, Paranal, Chile - 60.A-9041

tion between the width and depth of the 1 micron spectral band and the topography (with respect to Vesta’s mean elevation) in regions near the South pole crater, supporting differentiation of Vesta mineralogy throughout its crust.

While much attention has been given to the mineralogical characterization of Vesta’s surface, little has been said about its color. The surface properties of Vesta – mainly the characteristics of its spectral signatures and relatively high albedo – suggest that its surface is somewhat protected from heavy space weathering [Hiroi et al., 1995]. However, recent laboratory experiments demonstrate that stronger spectral differences between Vesta and the HED meteorites should be expected [Marchi et al., 2005a; Vernazza et al., 2006]. Marchi et al. [2005a] and Vernazza et al. [2006] performed ion irradiation experiments on pyroxene and eucrite samples and found that their reflectance spectrum reddens with progressive irradiation. As those minerals are the main components of Vesta’s surface, one would expect solar-wind ions to redden its spectrum and lower its albedo.

The spectroscopic match between Vesta and the HED meteorites implies that either some processes rejuvenate its surface continuously, or that the action of the solar wind ions onto its surface is lower than expected. From the dynamical dispersion of the Vestoid members, we can infer that the impact event responsible of the southern crater has occurred more than 1 Gyr ago [Marzari et al., 1996; Nesvorný et al., 2008], which is longer than the timescale needed for space weathering to alter Vesta’s surface properties [Brunetto et al., 2006; Vernazza et al., 2006, 2009]. Recently, Shestopalov and Golubeva [2008] proposed that continuous bombardment of Vesta’s surface by small meteors could be a possible mechanism to rejuvenate its surface. They propose that numerous small-sized debris ejected during the large southern impact may have remained within the gravitational sphere of influence of Vesta. Close encounters with other minor planets would then trigger instabilities resulting in those fragments to fall onto Vesta, thus mixing its regolith and erasing the space weathering effects. However, the quantity of debris and their orbital timescale remain to be evaluated. Vernazza et al. [2006] suggested an alternative mechanism. They showed that a remnant magnetic field of only  $\sim 0.2$  micro-Tesla ( $\mu\text{T}$ ) could shield a large portion of Vesta’s surface from solar wind ions, explaining at once Vesta’s largely unweathered aspect and strong color variations (from the presence of magnetic “cusps”).

Here we report the first ground-based disk-resolved spectral study of an asteroid surface. The near-IR mapping of Vesta’s spectral slope and absorption bands properties allowed us to investigate possible causes for their spatial variations, such as heterogeneity in its surface composition or in the strength of space weathering [Brunetto et al., 2006].

## 2. Observations and Data Reduction

### 2.1. SINFONI

Vesta was observed with the Spectrograph for INtegral Field Observations in the Near Infrared (SINFONI) [Bonnet et al.,

**Instrumental Settings**

Grating	$\lambda$ ( $\mu\text{m}$ )	$\lambda/\Delta\lambda$	Pixel scale (mas/pix)	FoV (arcsec <sup>2</sup> )
<i>J</i>	1.10-1.40	$\sim 3000$	$25 \times 12.5$	$0.8 \times 0.8$
<i>H+K</i>	1.45-2.45	$\sim 1500$	$25 \times 12.5$	$0.8 \times 0.8$

Table 2: Wavelength range ( $\lambda$ ), spectral resolution ( $\lambda/\Delta\lambda$ ), pixel scale (in milli-arcsecond per pixel) and size of the field of view (FoV) for each spectroscopic mode used in this study.

2004] during the 2004 science verification campaign (Prog. ID: 60.A-9041) of the instrument. SINFONI is mounted on the cassegrain focus of the Yepun telescope (UT4) at the European Southern Observatory’s (ESO) Very Large Telescope (VLT). SINFONI’s main sub-systems are the Adaptive Optics (AO) module (Multi-Application Curvature Adaptive Optics: MACAO) developed at ESO [Bonnet et al., 2003], and the integral-field unit (SPectrometer for Infrared Faint Field Imaging: SPIFFI) developed at the Max Planck Institute for Extraterrestrische Physik (MPE) in collaboration with Nederlandse Onderzoekschool Voor Astronomie (NOVA) and ESO [Eisenhauer et al., 2003]. An “image slicer” cuts the field of view (FoV) into 32 image-slitlets, which are redirected towards the spectrograph grating, to be re-imaged onto a  $2048 \times 2048$  pixels Hawaii 2RG detector. The original FoV is reconstructed into an  $64 \times 64$  pixel image-cube, each slice of the cube corresponding to an image of the FoV at a given wavelength. Fig. 1 presents an example of a reconstructed image.

### 2.2. Observations

We observed Vesta at three epochs: 2004 August 21, August 23 and October 4 (Table 1), one month apart from Vesta’s opposition (2004, September 13 UT). Data obtained on August 23 were impacted by poor seeing conditions and were thus discarded from our analysis. We used the highest angular-resolution provided by SPIFFI with an equivalent pixel size on sky of  $25 \times 12.5$  milli-arcsec and a resulting field of view of  $0.8 \times 0.8$  square arcseconds. Image-cubes were obtained across the  $[1.1-2.4] \mu\text{m}$  range with the *J* and *H+K* gratings (Table 2).

### 2.3. Data reduction

We reduced the SINFONI data with the ESO data-reduction pipeline (version 1.8.2). At the time of the observations, the instrument was equipped with an engineering-grade detector [Bonnet et al., 2004], suitable for technical qualification but that had a large defect affecting the data quality after 1.35 and  $2.4 \mu\text{m}$  for the *J* and *H+K* grating respectively. The *J* observations also presented higher noise at short wavelengths and we had to discard the 1.1-1.17 micron range. Distance and distortion calibration tables were provided by the commissioning team [H. Bonnet, private communication]. Basic calibrations (dark frames, lamp flats, and Ar and Xe lamps for the wavelength calibration) were obtained via SINFONI calibration plan. Each objet-sky pair of frames were reduced using the pipeline to correct from bad pixels, flat-fielding, sky subtraction and reconstruct the image-cubes.

### Observing Conditions

Date (UT)	Grating	$\Delta$ (AU)	$r$ (AU)	$\alpha$ ( $^\circ$ )	$\phi$ ( $''$ )	SEP $_\lambda$ ( $^\circ$ )	SEP $_\varphi$ ( $^\circ$ )	X	Seeing ( $''$ )	$\Theta^\dagger$ ( $''$ )	(km)
2004 Aug 21 - 04:59	<i>H+K</i>	2.35	1.41	12	0.55	179	-15	1.13	1.1	0.084	144
2004 Aug 21 - 08:28	<i>J</i>	2.35	1.41	12	0.55	304	-15	1.14	1.1	0.218	371
2004 Aug 21 - 08:46	<i>H+K</i>	2.35	1.41	12	0.55	285	-15	1.18	1.2	0.084	144
2004 Oct 04 - 00:20	<i>J</i>	2.39	1.45	11	0.53	240	-15	1.34	0.5	0.053	92
2004 Oct 04 - 00:33	<i>H+K</i>	2.39	1.45	11	0.53	226	-15	1.29	0.5	0.055	95

Table 1: Vesta’s heliocentric ( $\Delta$ ) and geocentric ( $r$ ) distances, phase angle ( $\alpha$ ), angular diameter ( $\phi$ ) and Sub-Earth Point (SEP) coordinates\* (longitude  $\lambda$  and latitude  $\varphi$ ) for each epoch (given in UT). Airmass (X), seeing and corresponding resolution element ( $\Theta$ ) at 1.2 and 2.2 micron (for the *J* and *H+K* grating respectively) in arcseconds on sky and kilometers on Vesta’s surface, are also reported for each observation. The poor spatial resolution obtained with the *J* grating in August is due to the poor meteo conditions that prevailed at that time. The data are available since December 2004 on the [ESO archive](#), under the program ID: 60.A-9041.

$^\dagger$ evaluated on the solar analog spectro-cubes.

\*coordinate system is planetocentric [IAU recommendation: [Seidelmann et al., 2007](#)]

### Solar Analogs

Designation	RA (hh:mm:ss)	DEC (dd:mm:ss)	Spectral Type	Mv (mag.)	Date (UT)	Filter	Airmass
HD 1835	00:22:52	-12:12:34	G5V	6.4	2004 Aug 21 - 05:35	<i>H+K</i>	1.10
HD 1835	00:22:52	-12:12:34	G5V	6.4	2004 Aug 21 - 09:06	<i>J</i>	1.17
HD 1835	00:22:52	-12:12:34	G5V	6.4	2004 Aug 21 - 09:13	<i>H+K</i>	1.19
HD 1461	00:18:42	-08:03:11	G0V	6.5	2004 Oct 04 - 00:54	<i>H+K</i>	1.52
HD 1461	00:18:42	-08:03:11	G0V	6.5	2004 Oct 04 - 01:04	<i>J</i>	1.45

Table 3: Solar analogs observed in this study, along with their equatorial coordinates, spectral type and visual magnitude (Mv). The UT time of observation, the filter and the airmass are also reported.

Due to atmospheric differential refraction, the position of the object across the cube slowly drifts with the wavelength. We thus re-aligned each slice of the image-cubes for both the solar analogs and Vesta. Solar analogs were also observed to correct our reflectance Vesta spectra from atmospheric absorption and solar color. The spectra of Vesta, and of the solar analog observed at similar airmass (see Table 3), were then extracted using an aperture compromising the maximum flux collected and the minimum residual sky contribution. Also, because the small FoV of SINFONI ( $0.8'' \times 0.8''$ ) caused some light to be lost in the wings of the PSF under poor seeing conditions, which had the effect of introducing an artificial slope in our solar analog spectra (see Fig. 2), we adjusted both the aperture size and the overall spectral slope of our solar analog to match Vesta’s disk-integrated spectrum [from [Vernazza et al., 2005](#)] (Fig. 3). This process also permitted to correct for any artificial slope possibly introduced by different atmospheric extinction between Vesta and the solar analogs observation. However, given this slope correction, we do not present absolute measurements of the spectral slope nor of Vesta’s composition. But since we processed the different data sets in a similar way, they are *self-consistent* and we can use them to study variations on Vesta’s surface.

As already addressed by several authors [e.g. [Binzel et al., 1997](#)], the grazing viewing angle affecting the region near Vesta’s limb causes unreliable flux measurement for the outer annulus of the asteroid’s apparent disk. We thus limited our

study to a restricted region of interest (ROI) covering the innermost portion of the disk. The ROI was defined by Vesta’s projected shape reduced to a given fraction [[Carry et al., 2008](#)], corresponding to a ROI of 60% of Vesta’s radius. We show the spectra in both wavelength ranges for each rotational phase in Fig. 4 and Fig. 5. Spectra are normalized to unity at  $1.17 \mu\text{m}$  and  $1.5 \mu\text{m}$  for the *J* and *H+K* gratings respectively; and smoothed with a median filter, using a box size of 8 pixels in the spectral direction for each spaxel.

### 3. Pyroxene Distribution

We present a mineralogical study of Vesta based on the analysis of spatially resolved reflectance spectra in the *H+K* range, and by looking for correspondence between regions of Vesta surface and HED subclasses and pyroxene minerals (orthopyroxene, clinopyroxene).

Pyroxene spectra are characterized by broad absorption bands centered at 1 and  $2 \mu\text{m}$ . The wavelength position of these absorption features constrains the nature of the minerals [[Adams, 1974](#)]. In our case, the telluric absorptions strongly affected the central region of the *H+K* range (Fig. 1), preventing a detailed investigation of pyroxene compositional variations across Vesta’s surface. However, one can still perform first level characterization of the pyroxene composition as the intensity of the slopes of the upward and downward  $2 \mu\text{m}$  absorption band are directly related to the detailed chemical con-

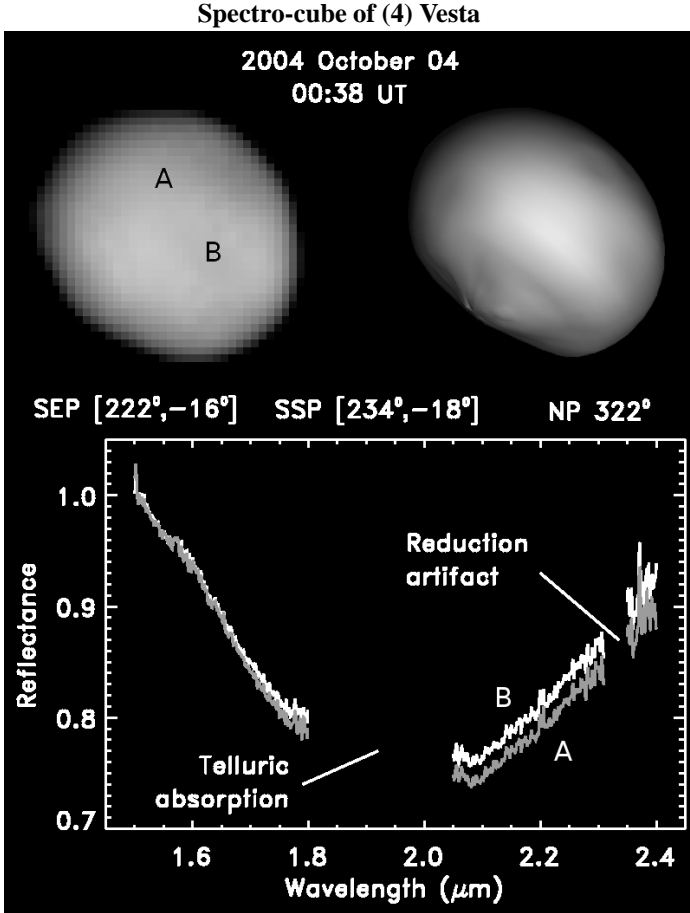


Figure 1: *Top left*: Image of Vesta obtained with the  $H+K$  grating for the 2004 October 04 UT run, by stacking all images of the cube along the wavelength direction. Orientation is usual with North up and East left. *Top right*: The shape model of Vesta at the same orientation [as defined by [Thomas et al., 1997b](#)] is given for comparison (model obtained from the Eproc ephemeris generator (<http://www.imcce.fr>)). We report the Sub-Earth Point (SEP) and Sub-Solar Point (SSP) coordinates (longitude, latitude) as well as the pole angle (NP: defined as the angle in the plane of the sky between the celestial north and the projected asteroid spin-vector, measured counter-clockwise, from North through East).

*Lower panel*:  $H+K$  spectra of two arbitrary selected spaxels A and B. We normalized all the spectra to unity at  $1.5 \mu\text{m}$  within this range and we degraded the spectral resolution to improve the signal-to-noise ratio by smoothing the spectra with a 8-pixel box median filter. We removed some artefacts around  $2.33 \mu\text{m}$  that contaminated our image-cubes.

This figure illustrates the peculiarity of a spectro-cube: it is a three dimensional array where each spaxel in the spatial plane is a spectrum in the third dimension.

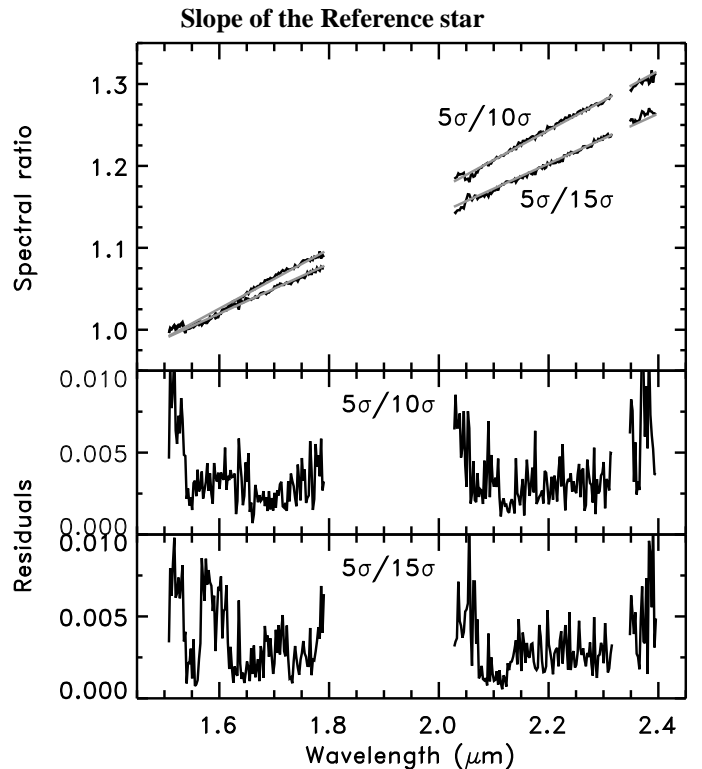


Figure 2: Ratio of the reference star spectrum (HD 1835 obtained in August, see [Table 3](#)) to itself, for several apertures (corresponding to 5, 10 and 15 times the standard deviation of the star) over the  $H+K$  wavelength range. For each ratio, we computed its linear regression, and show the deviation (residuals) to this linear fit in the two lower panels. According to the chosen aperture a strong linear slope over the wavelength range is introduced. We corrected this effect by dividing the stellar spectra by linear function (see text), whose slope were adjusted to match previous observations of Vesta [[Vernazza et al., 2005](#)].

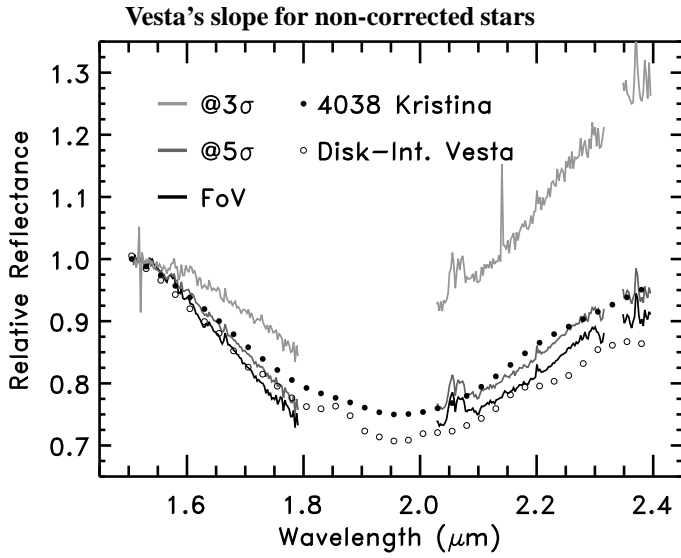


Figure 3: Following Fig. 2, we show some disk-integrated spectra of Vesta obtained without the linear correction of the stellar spectra and for several aperture values (FoV meaning integrating the flux over the whole FoV). We show for comparison in open circles the spectrum of Vesta obtained with long slit spectroscopy by Vernazza et al. [2005], and in filled circles the very red small Vestoid (4038) Kristina (see section 5.1 for more info on this asteroid). This figure clearly shows the need for correcting the stellar spectrum slope (see text).

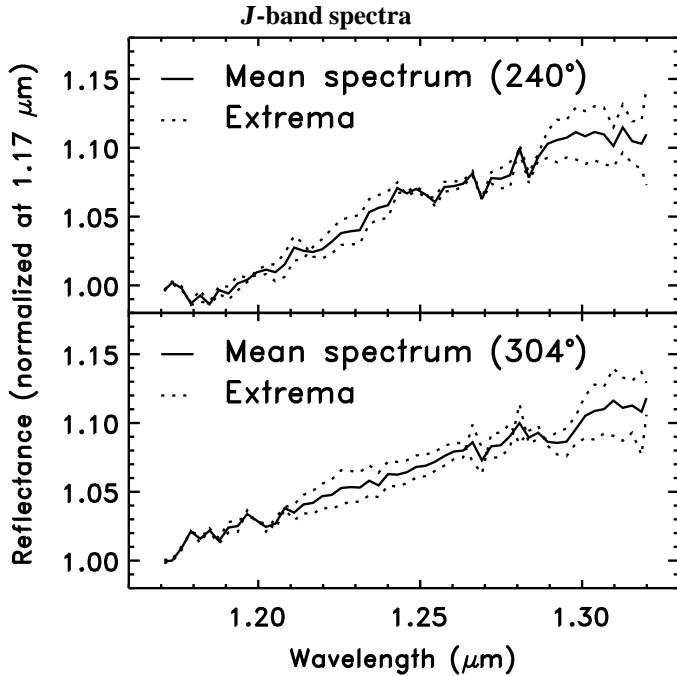


Figure 4: Average (solid line) and envelope spectra (dotted lines) obtained with the *J* grating normalized to unity at  $1.17 \mu\text{m}$ . Each panel corresponds to a different rotational phase as reported on the figure (see Table 1). The slope heterogeneity across Vesta's surface is visible from the breadth of the envelopes at long wavelengths (see section 4).

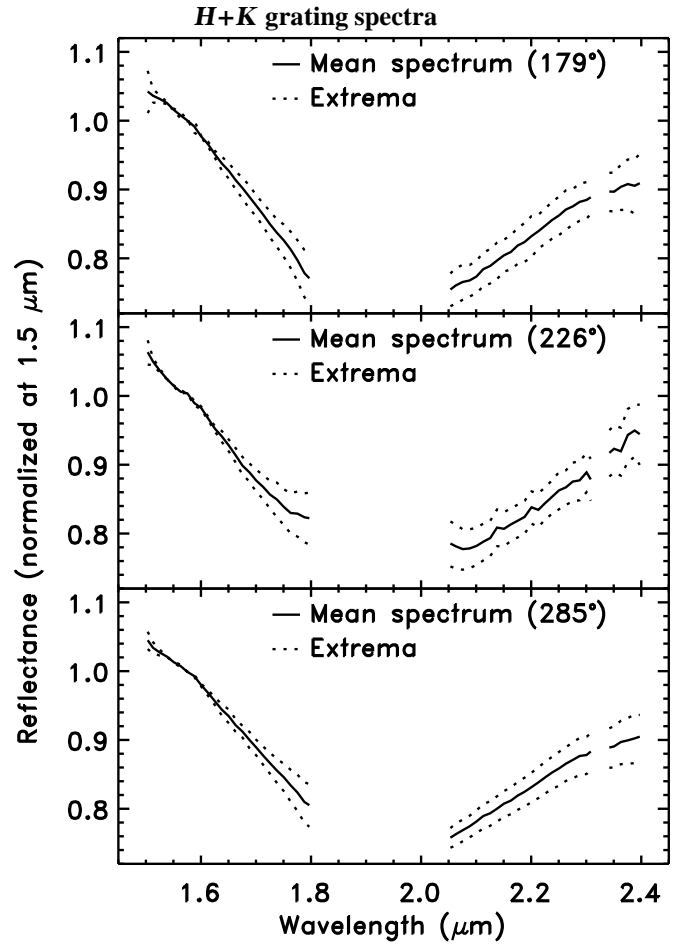


Figure 5: Average and envelope spectra obtained with the *H+K* grating normalized to unity at  $1.5 \mu\text{m}$ . Each panel corresponds to a different rotational phase of Vesta as reported on the figure (see Table 1). Vesta's surface properties heterogeneity is visible from the breadth of the envelopes longward of  $1.8 \mu\text{m}$ .



tent of the pyroxenes. A gradual downward slope associated with a steep upward slope indicate a position of the band center shifted towards short wavelengths. The absorption shifts towards short wavelengths for low calcium pyroxenes (*i.e.* orthopyroxene), while the opposite is true for high calcium pyroxenes (*i.e.* clinopyroxene). For HED meteorites, the absorption is positioned at short wavelengths for diogenites, and increases for the howardites and eucrites [Gaffey, 1997]. This trend appears clearly from average HED spectra: we computed the average spectra for the howardite, eucrite and diogenite meteorite classes, using 20, 20 and 76 samples (from RELAB: <http://www.planetary.brown.edu/rellab/>) respectively; we also computed the average spectrum for augite (high calcium clinopyroxene, 6 samples). These mean spectra, scaled to unity at 1.5  $\mu\text{m}$ , are shown in Fig. 6, after removal of the overall HK-bands spectral slope. This was done by fitting and removing a linear continuum between 1.5  $\mu\text{m}$  and 2.4  $\mu\text{m}$ . Figure 6 shows that the diogenites absorption (almost pure orthopyroxene) is located at shorter wavelength than the howardites (mixture of diogenites and eucrites) and eucrites (mainly clinopyroxene). Similarly, the steepest slope for upward band is seen for diogenites, followed by howardites and eucrites, which agrees with band center calculations for these meteorite classes [Gaffey, 1997]. We tested further this mineralogical determination by modeling the mean howardite spectrum using a mixture of eucrites and diogenites as end-members (see Fig. 7). The best fit of the howardite band was reached for a  $\sim 2/3$  -  $1/3$  mixing ratio of eucrite and diogenite, demonstrating the validity of this technique based on the analysis of the upward and downward slopes of the pyroxene absorption band.

The next step consisted in performing a direct comparison of our spectra of Vesta with the laboratory spectra presented above. Each spectrum of Vesta was computed as the mean of all within a region defined by the system's resolution element, and weighted by a Gaussian function with standard deviation equal to the AO-corrected seeing at the time the observations were made (Table 1). We display these average spectra of Vesta after slope removal in Fig. 6.

Prior to fitting each average spectrum of Vesta by a linear combination of the mean eucrite and diogenite spectra, we applied a chi-square fit between the meteorites' band depth and that of Vesta to compensate for grain size differences between Vesta's surface and the meteorite samples. We present in Fig. 8 two examples of these fits.

We find that Vesta's spectra are quite homogeneous with varying longitude, which was expected from the report by Binzel et al.'s [1997] of constant position of the 1 micron band over our longitude range. This reveals a roughly homogeneous composition across our observed regions, mostly compatible with howardite meteorites (mix of about 2/3 of eucrite with 1/3 of diogenite, see Fig. 7 and Fig. 8). However, we note a North-South trend, with the amount of diogenite increasing towards Southern longitudes, up to 50% diogenites at  $\text{lat}=-50^\circ$ . We also note a higher concentration of diogenite-like material around ( $180^\circ$ ,  $-25^\circ$ ), with the diogenite ratio increasing up to 76%. It is interesting to note that based on spectrophotometric observations of Vesta at different rotational phases, Gaffey [1997] had

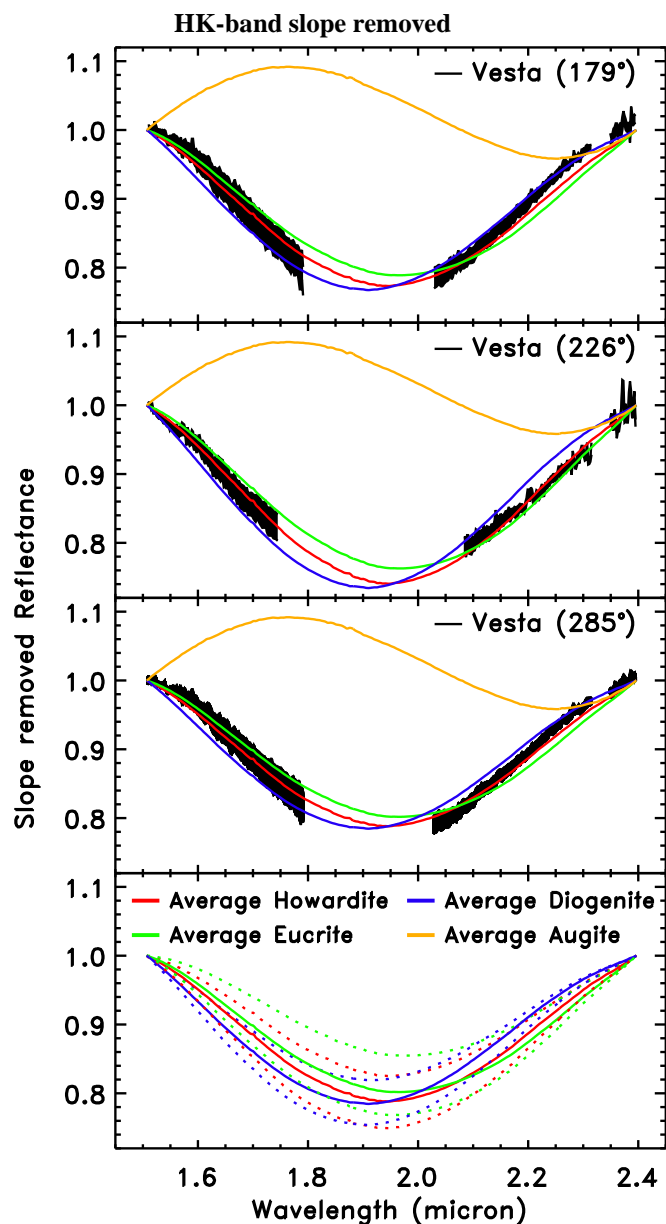


Figure 6: Vesta's spectra for the three  $H+K$  observations after HK-band spectral slope removal (see text). For each data-set, we overplot the average HED and augite spectra (based on 20, 76, 20 and 6 samples respectively) after slope removal. The lowermost panel represents the HED meteorites spectra with their standard deviation shown as dotted lines. The latter one is strongly affected by slope and grain size hiding the influence of mineralogy. Although the classes overlap close to the band center, they are separable near the band ends. From the global band shape at each rotational phase, one can already see that the Vesta's spectra above will neither match pure eucrite nor pure diogenite composition, but a mix of these minerals instead.

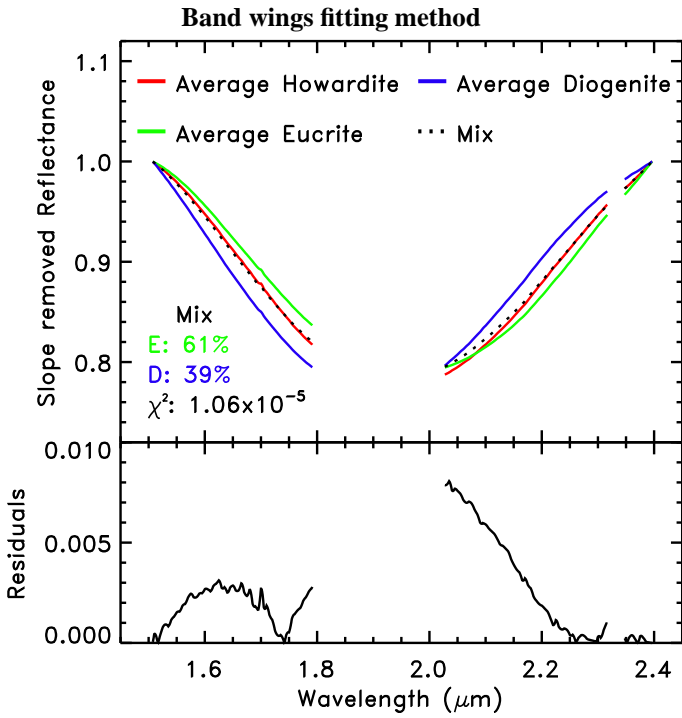


Figure 7: We present here the method used to determine Vesta's mineralogy in terms of mixing ratios of eucrites and diogenites. The upper panel shows the average spectra of the howardite, eucrite and diogenite meteorites used in this study. We fit the howardite spectrum with a combination of 61% of eucrite and 39% of diogenite, The fit residuals are showed in the lower panel. Although the choice of end-members in our fit is likely not unique, the low level of residuals obtained indicates that this technique can be used as a good approximation to study Vesta mineralogy.

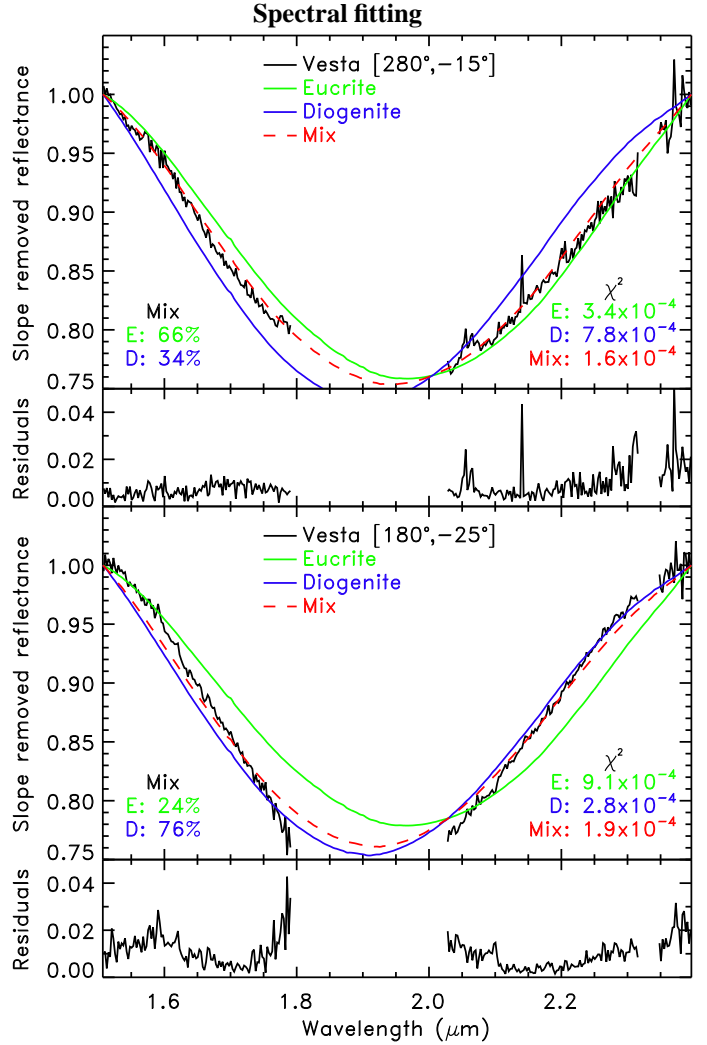


Figure 8: Spectra of the eucrites and diogenites used to fit the spectrum of Vesta for two distinct areas of the asteroid. We report the chi-square values ( $\chi^2$ , bottom-right corner) for each meteorites and for the model whose mixing ratios are given at the bottom-left corner of each figure. The residuals of the fit are shown at the bottom of each figure. The upper panel shows that Vesta's surface near (lon=280°, lat=-25°) can be best modeled with a mixture of about 2/3 of eucrite and 1/3 of diogenite (howardite-like material). Lower panel represents the best fit ( $\chi^2$  almost a factor of two better than if using the same mixture as elsewhere). for a small diogenite-rich area (1/4 of eucrite and 3/4 of diogenite) located around (180°, -25°). Our analysis shows a North-South trend in terms of percentage of diogenites, which increases Southward, up to 50% of the mixture.

reported a diogenite-like spot around this longitude. This disk-resolved spectroscopic observations allows us to locate this spot at southern latitudes.

Finally, none of our spectra can be modeled with the spectrum of augite, suggesting a lack of clinopyroxene-rich (high calcium) area in the regions observed in this study.

#### 4. Spectral slope of (4) Vesta

The continuum slope displayed by Vesta's spectra over the visible and near-infrared range (VNIR) can be function of the mineralogy, the scattering properties of the surface (grain size, surface roughness) and/or by the space weathering. Here, we present an analysis of the information that can be derived from the spectral slope of our data-set, and further discuss possible implications. We restrict our analysis to the 1.17-1.32  $\mu\text{m}$  range (*J* grating) because mineralogical variations across Vesta can modify the width of the 2-micron band.

For each image-cube, we measured the spectral slope of each resolution element as a function of the central spaxel (similarly to what we did for the *H+K* observations, see section 3 and see also Table 1 for the size of the resolution element:  $\sim 90\text{-}370\text{km}$ ). Then we reported the slopes and diogenite mixing ratios values onto an Equidistant Cylindrical Projection map (Fig. 9) [see Carry et al., 2008, for details]. Although our spatial analysis is hampered by the sometimes large value of the resolution element, we find the Eastern part of Vesta (limited by the  $260^\circ\text{E}$  meridian) being slightly redder (sloped of  $\sim 0.6$  to  $0.8$ ) than the Western regions (slopes of  $\sim 0.5$  to  $0.7$ ). It is important to note that the uncertainties on the slope values are negligible with respect to their relative variations, although the absolute slope values might be biased (section 2.3). This result agrees with previous reports that the Eastern regions of Vesta display a redder spectral slope in the visible, based on disk-integrated spectroscopy [Fig. 5 in Gaffey, 1997], ultra-violet light-curves [Fig. 1 in Hendrix et al., 2003] and disk-resolved imaging [A and B features in Fig. 3 of Binzel et al., 1997].

We also carried out a comparative study of the diogenites abundance, spectral slope, visible albedo [Li et al., 2008], and the topography of Vesta [elevation map of Thomas et al., 1997a] and showed that these quantities have apparently no correlation with each other (correlation coefficients are 0.07, 0.22 and -0.04 between the composition and the slope, the albedo and the topography respectively). Similarly, no correlation was found between the albedo distribution across the regions of Vesta we observed, and their corresponding topography (correlation coefficient of -0.13). Nevertheless, two trends seem to emerge from our data. Low altitude regions display redder spectra (correlation coefficient of -0.6), which also seem to be found (slope  $\geq 0.7$ ) primarily in low albedo regions (correlation coefficient of -0.3).

## 5. Discussion

In summary, Vesta's surface display a high albedo [Binzel et al., 1997; Zellner et al., 2005] and strong spectral slope variations [Binzel et al., 1997, and current study] in the visible and near-infrared range. Over the small area observed in this study, it is unlikely that these variations be due to a variation of the composition. However, since the wavelength range we covered is limited we cannot definitely discard a compositional origin for both the slope and/or albedo trends [although disk-integrated observations did not report VNIR spectral inhomogeneity across these longitudes, see Gaffey, 1997]. The present study seems to support that spectral slope is somewhat linked to the topography and the albedo.

### 5.1. Should (4) Vesta be space weathered?

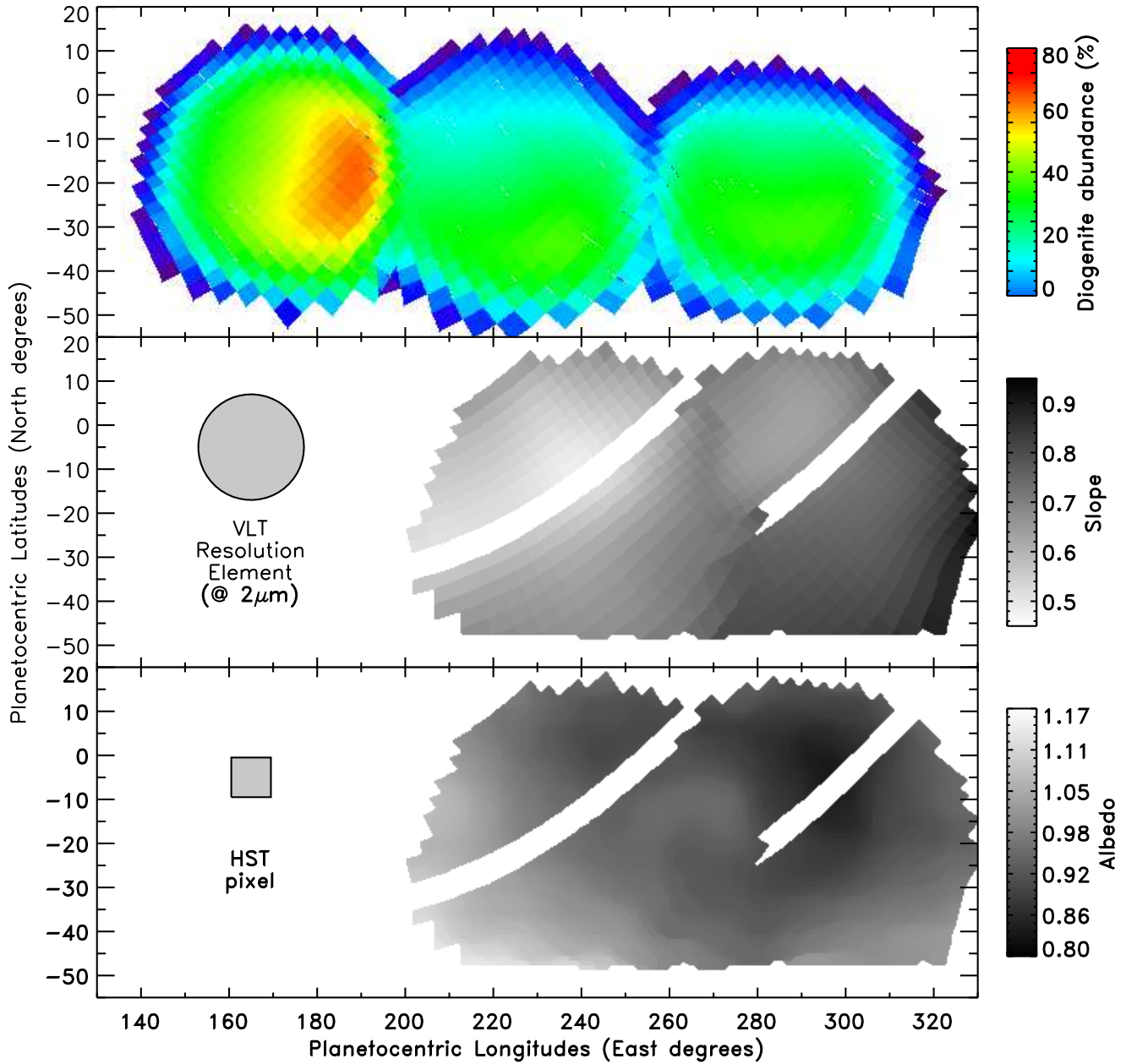
The surface of the Solar System bodies that are not protected by an atmosphere or a magnetosphere are exposed to the stream of impacting solar ions. The effects of continuous bombardment by solar wind ions and interplanetary dust (so called "space weathering") have been studied to improve our understanding of the connections between the spectral properties of meteorites and the remote sensing data of asteroids. Indeed, as demonstrated by laboratory experiments, space weathering can explain the spectral mismatch between the most populous class of meteorites (ordinary chondrites, OC) and the surface spectra of their presumed (S-type) asteroidal parent bodies [Pieters et al., 2000; Sasaki et al., 2001; Marchi et al., 2005a; Strazzulla et al., 2005], while it also explains the spectral difference between lunar soils and underlying rocks [Pieters et al., 2000; Blewett et al., 2007].

Using laboratory measurements, Vernazza et al. [2006] exposed the Bereba meteorite (eucrite), thought to originate from Vesta, to ion bombardments and showed that, Vesta should be substantially more weathered than it appears (*i.e.* its reflectance spectrum should be much redder and its albedo lower), as already addressed in the past [*e.g.* Chapman, 2004]. To strengthen this important point, we represented an albedo-slope diagram for Vesta (Fig. 10) (visible data from SMASS [Bus and Binzel, 2002], NIR data from Vernazza et al. [2005]). Earlier studies of Vesta [*e.g.* McCord et al., 1970] revealed that its primary surface components are very similar to those of the HED meteorites. We also included in the diagram the achondrite HED meteorites (using the reflectance at  $0.55 \mu\text{m}$  as visible albedo) used within this study (see section 3). We illustrate the space weathering action on HED assemblages by plotting together with Vesta and the HED, the small Vestoid (4038) Kristina – a Vw-type (weathered) asteroid [see the taxonomy by DeMeo et al., 2009] (visible data from SMASS, NIR data from R. P. Binzel [personnal communication]) –, and the eucrite Bereba [from Vernazza et al., 2006] before ( $B_0$ ) and after irradiation ( $B_1$ ).

We first search for a trend between the slope and the visible albedo (reflectance at  $0.55 \mu\text{m}$ ) for HED meteorites. The correlation coefficient is 0.5 for howardite, 0.28 for eucrite and 0.14 for diogenite. Interestingly, even if these correlation values are



### Composition, Albedo and Slope Maps



[Li et al., 2008]

Figure 9: Comparison of the maps showing the diogenite abundance measured on Vesta (*Top*), the spectral slope (*Middle*) and the visible albedo (*Bottom*) [from HST, Li et al., 2008]. We report both HST pixel size [ $\sim 39$  km, Li et al., 2008] and VLT smallest resolution element on the albedo map. The diogenite abundance is nearly constant across the observed longitudes, with a small increase visible around ( $180^\circ$ ,  $-25^\circ$ ). The blue surroundings in the abundance map are artifacts related to the singularity at the disk border. The uncertainty of our abundance measurements is evaluated to be 10-20%, based on the analysis of overlapping areas. The diagonal stripes visible on the albedo and slope maps, corresponds to a noisy regions in our  $J$  grating data, which was removed from this analysis. The spectral slopes range from 0.5 to 0.8 (see also Fig. 4).

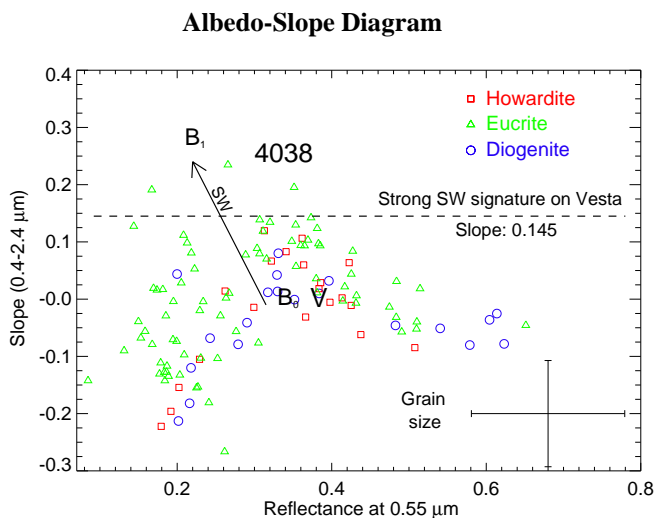


Figure 10: Spectral slope derived from the 0.4-2.4  $\mu\text{m}$  range against the absolute reflectance at 0.55  $\mu\text{m}$  (visible albedo) for the howardite (20), eucrite (76) and diogenite (20) meteorites cataloged in the RELAB spectral database. We also report the slope of the eucrite meteorite Bereba before ( $B_0$ ) and after ( $B_1$ ) irradiation [from Vernazza et al., 2006]. The effect of Space Weathering (SW) is symbolized by the black arrow. We also plot the slope and albedo of (4) Vesta (V: disk-integrated) and of the small Vestoid (4038) Kristina (see text). We stress that 4038’s albedo is yet unknown. The position of 4038 in the x-axis is therefore arbitrary. Because Vesta’s composition is found similar to the HED meteorites, and 97.5% of the HED meteorites available from RELAB are situated under the 0.145 slope limit (horizontal dashed line), we stress that any region on Vesta whose slope would be higher than 0.145 should be considered as affected by space weathering.

quite low (especially for eucrite and diogenite), they are positive. Note that space weathering (SW) would generate negative values (steeper slopes with lower albedo), like the one found here on Vesta.

Interestingly, the slope distribution of the HED meteorites allows us to define a slope limit over which one should consider certain that Vesta’s surface is space weathered. From our mineralogical investigation (see section 3), the primary surface component appears to be howardite-like material, in agreement with previous investigations [e.g. Gaffey, 1997]. We therefore draw an horizontal dashed line (Fig. 10; constant slope of 0.145) that highlights the highest slope value found for howardites (which is also an upper limit for diogenites). With such a limit, 97.5% of the HED meteorites available from RELAB are situated under the slope limit; only three meteorites, the eucrites Padvarninkai (MB-TXH-096-A), LEW87004 (MP-TXH-079-A) and Bouvante (MP-TXH-090-A) are redder.

We then remark that (4) Vesta and (4038) Kristina have a very different spectral slope (0.01 against 0.26) despite their similar composition (mostly similar to howardite/diogenite meteorites, see band analysis in Fig. 11). While Vesta’s slope lays in the middle of the HED slope domain, (4038) Kristina’s slope is situated well above that of any HED sample: the average spectral slopes for the three meteorite classes are  $-0.02$  for howardites,  $0.00$  for eucrites and  $-0.04$  for diogenites (with a standard deviation for each class of 0.10, 0.10 and 0.07). This result based on VNIR measurements supports earlier results based on visible measurements only [Hiroi and Pieters, 1998]. Interestingly, the difference between Vesta’s and 4038’s slope is extremely similar to the difference between Bereba’s slope before and after irradiation (see Fig. 10). This is indeed the case for all the Vestoids, whose spectral slopes are much higher than the HEDs’, and appear to be mostly similar to those of lunar soils [see Fig. 3 in Hiroi and Pieters, 1998]. Thus, the red slopes of the Vestoids, which are well above the mean slope for HED meteorites, show clearly that their surfaces are space weathered (with the same slope difference as observed between S-type asteroids and OCs). This also supports laboratory experiment results predicting that pyroxene-rich surfaces should redden in space [Marchi et al., 2005a; Vernazza et al., 2006], but do not solve the puzzling question about Vesta’s color: “why isn’t it red?”.

Two scenarios could explain at the same time the unweathered aspect of Vesta, its surface heterogeneity in both albedo and spectral slope, the relationships found between topography, albedo and spectral slope, and the weathered behavior of the Vestoids.

The first scenario implies regolith migration occasioned by seismic activities [Shestopalov and Golubeva, 2008] and the second predicts the existence of a remnant magnetic field on the surface of Vesta [Vernazza et al., 2006].

## 5.2. Seismic activities

As proposed by Shestopalov and Golubeva [2008], the dynamical relaxation of the south pole giant crater may induce long-term seismic activities. Asphaug [1997] had computed

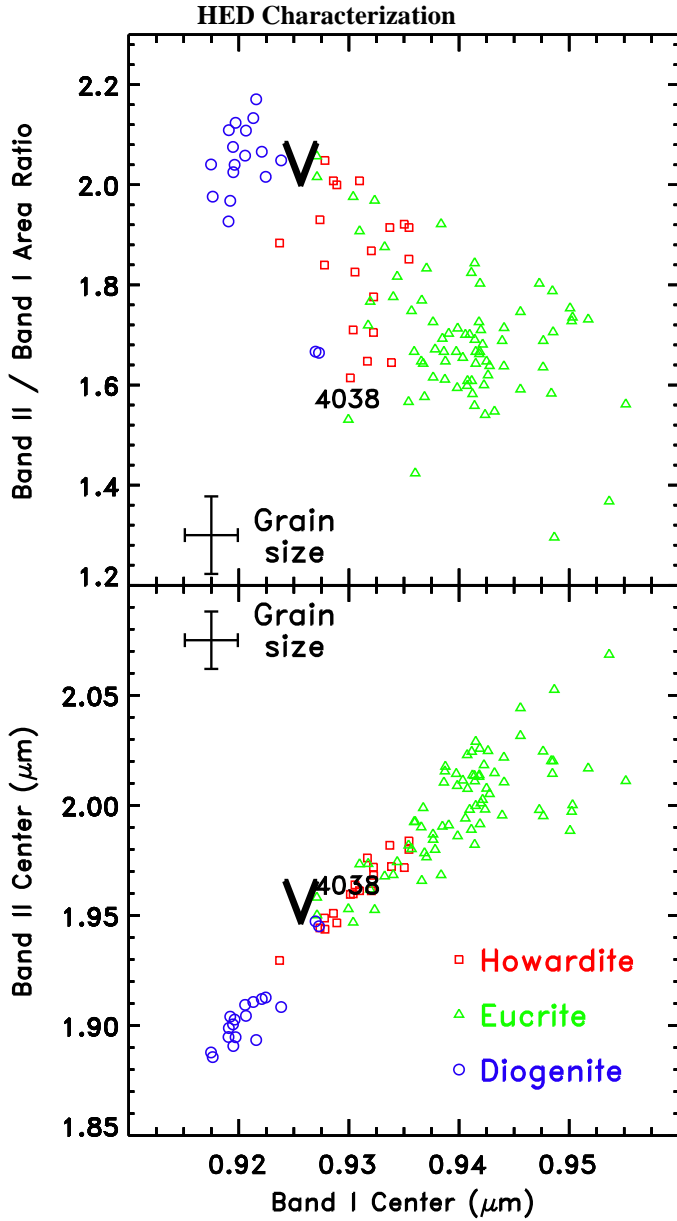


Figure 11: *Lower panel:* Pyroxene Band II center versus Band I center [following Gaffey et al., 2002] for HED meteorites present in the RELAB database (20, 20, 76 samples respectively). *Upper panel:* Band Area Ratio (BAR) versus Band I center for the same spectra. Since the RELAB spectral database stops at  $2.6 \mu\text{m}$ , the 2 micron band was not entirely covered for several samples, we may thus underestimate their BAR value. We also report the values for a disk-integrated spectrum of Vesta and for the spectrum of a the small Vestoid (4038) Kristina, allowing rough composition determination, here mainly howardite and diogenite like Vesta. RELAB samples are available for several grain sizes, we thus report the standard deviation of these quantities due to the grain size effect.

a dynamical time of about  $6 \times 10^8$  yrs (the computation depends on Vesta’s crust viscosity for which we can have only a crude estimate). This means that these activities may still happen nowadays. An effect of the seismic activity could be a sorting of the regolith, with landslides toward lower altitude regions. Thus, the weathered regolith would accumulate in low altitude regions while fresh regolith would be continuously revealed in upper altitude regions. This would explain the relationship found here between the spectral slope and the topography, as well as the surface heterogeneity of Vesta and its overall unweathered aspect. Last point, such activity is not expected on the Vestoids and this scenario is thus compatible with their colors.

There are two major drawbacks to this scenario namely 1) the lack of correlation found between the albedo markings and the topography and 2) the age of the crater. For the first point, in the hypothesis of regolith sorting, the weathered material would be located in low altitude regions (suggested by the correlation between spectral slope and topography). If true, we should also observe a correlation between the albedo and the topography while we do not. The other point concerns the time of formation of the south pole crater. Dynamical simulations that link Vesta family members to Vesta itself require a  $\sim 1$  Gyr timescale [Marzari et al., 1996; Carruba et al., 2005] This timescale exceeds the dynamical relaxation timescale by a factor of 2 at least.

### 5.3. Magnetic field

Vernazza et al. [2006] have suggested the presence of a fossilized magnetic field inside magnetized blocks of crustal material on Vesta. With just a minimum strength  $0.2 \mu\text{T}$  (value similar to the Moon’s local-crustal magnetic fields, a few hundred times smaller than Earth’s own field), such a magnetic field could effectively deflect the solar wind ions. The result would be a succession of localized crustal magneto-spheres where the solar wind particles would reach the surface via a number of “cusps”. This scenario implies the presence of several dark and bright regions, associated to spectral slope variations [following the trend of irradiated pyroxene as described in Marchi et al., 2005a; Brunetto et al., 2006]. Such a behavior has already been observed on the Moon, in absence of topography, where bright (solar wind protected?) areas (called “swirls”) have been found within dark (solar wind unprotected) maria [e.g. Blewett et al., 2007; Richmond and Hood, 2008, and reference therein].

An objection to this scenario would be the fact that the Vestoids, being ejecta from Vesta’s crust, should also possess a remnant magnetic field and may thus be protected from the effect of the solar wind. In fact, Vestoids are not expected to be preserved from the solar wind action even if they possess a remnant (or fossile) magnetic field. This is due to the fact that the intensity of a magnetic field decreases with the third power of the body’s dimension, and given the Vestoids’ small sizes ( $D < 10$  km), the required magnetic field strength to protect their surface should be much higher (a factor of about 1000) than the one needed in Vesta’s case ( $0.2 \mu\text{T}$ ). It thus appears very unlikely that Vestoids will be protected against the weathering effect of the solar wind.

#### 5.4. Observing limitations

The analysis and conclusion presented here are limited by several observing constraints:

**Spectral range:** The spectral slope used here was calculated over a very short wavelength range (1.17-1.32  $\mu\text{m}$ ), and our mineralogical analysis was limited to the (1.5-1.8  $\mu\text{m}$  and 2.05-2.4  $\mu\text{m}$ ) region of the spectrum. As a result, we cannot fully discard a compositional origin for the slope and/or albedo trends seen on Vesta (although the longitude range observed here has been reported to be of homogeneous composition [Gaffey, 1997]).

**Spatial resolution:** Both albedo and spectral slope maps are limited by “macroscopic” spatial resolution (tens of kilometers). For instance, the low spatial resolution of our August data (Eastern areas) hamper strongly our ability to detect any spatial variation, thus leading to a roughly uniform  $\sim 0.7$  slope across Vesta’s surface. More important, the still limited spatial limitation does not allow us to check (1) any topographic origin (e.g. fresh crater, high sloped terrain) of these bright marking, and (2) the fine structure morphology of Vesta’s bright markings which could be identified at the presence of swirls [from their peculiar shape, see Blewett et al., 2007]. Note that the largest lunar swirl (Reiner Gamma Formation) is about the same size ( $87 \times 110$  km) as our smallest resolution element ( $90 \times 90$  km).

**Observed area:** Our observations only covered the region around  $260^\circ\text{E}$ , which corresponds to Vesta’s “dark” hemisphere [see Binzel et al., 1997; Hendrix et al., 2003; Li et al., 2008]. To better characterize the relationship between slope and albedo, this spectroscopic observations should cover Vesta’s brightest and darkest markings.

Given these remarks, we can only suggest putative correlations between (a) spectral slope and topography and (b) spectral slope and albedo. We suggest that our results are unlikely due to composition variation, but instead to competing processes inhibiting/erasing the effect of the space weathering on Vesta [Binzel et al., 1997]. Neither the spectral coverage (1.17-1.32  $\mu\text{m}$  for the slope), the spatial resolution ( $\geq 100$  km) nor the spatial coverage (14% of Vesta’s surface), allow us to conclude with confidence about the mechanisms at stake in keeping Vesta surface so young.

Nevertheless, a similar analysis applied to higher spatial-resolution data covering a larger spectral range, like the Dawn mission will provide, will certainly help to shed light on the action of space weathering onto Vesta.

## 6. Conclusion

We presented the first disk-resolved spectroscopic observations of an asteroid surface from the ground. We observed (4) Vesta in the near-infrared (1.1-2.4  $\mu\text{m}$ ) with SINFONI on the ESO Very Large Telescope by combining the high angular resolution (about  $0.050''$  at best) provided by Adaptive Optics, with

the moderate spectral resolution ( $\lambda/\Delta\lambda \geq 1500$ ) of its integral-field unit. Our observations covered only a small fraction of Vesta’s surface (about 16% and 23% for  $J$  and  $H+K$  observations respectively) with an equivalent spatial resolution down to  $\sim 90 \times 90$  km. Vesta’s composition is found to be mostly compatible with howardite meteorites, although the presence of a small spot of diogenite is suggested around  $\text{long}=180^\circ\text{E}, \text{lat}=-25^\circ\text{S}$  (the spectral coverage presented here is not sensitive to olivine).

We have investigated the relationship between the spatial distribution of NIR spectral slopes and visual albedo, and found that the near-infrared spectral slopes might vary inversely with the albedo. Such a trend would support Binzel et al. [1997]’s findings, based on imaging observations performed with the HST in the visible. We also found that low altitude regions appear to display redder spectral slopes, supporting a possible regolith migration on Vesta’s surface. However, given our limited spatial resolution and coverage, these results have to be considered as preliminary, rather than reliable conclusions.

## Acknowledgments

Thanks to L. A. McFadden, J.-Y. Li and P. C. Thomas for sharing the albedo and elevation maps of (4) Vesta from HST observations. Thanks also to R. P. Binzel for providing (4038) Kristina near-infrared spectrum and to H. Bonnet for the SPIFFI distortion and distance tables obtained during SINFONI commissioning. We would like to thank one of our referees whose comments greatly helped to improve the manuscript.

## References

- J. B. Adams, 1974. Visible and near-infrared diffuse reflectance spectra of pyroxenes as applied to remote sensing of solid objects in the solar system. *Journal of Geophysical Research*, 79:4829–4836.
- E. Asphaug, 1997. Impact origin of the Vesta family. *Meteoritics and Planetary Science*, 32:965–980.
- R. P. Binzel, M. J. Gaffey, P. C. Thomas, B. H. Zellner, A. D. Storrs, and E. N. Wells, 1997. Geologic Mapping of Vesta from 1994 Hubble Space Telescope Images. *Icarus*, 128:95–103.
- R. P. Binzel, A. S. Rivkin, J. S. Stuart, A. W. Harris, S. J. Bus, and T. H. Burbine, 2004. Observed spectral properties of near-Earth objects: results for population distribution, source regions, and space weathering processes. *Icarus*, 170:259–294.
- R. P. Binzel and S. Xu, 1993. Chips off of Asteroid 4 Vesta: Evidence for the parent body of basaltic achondrite meteorites. *Science*, 260(5105):186–191.
- D. T. Blewett, B. R. Hawke, N. C. Richmond, and C. G. Hughes, 2007. A magnetic anomaly associated with an albedo feature near Airy crater in the lunar nearside highlands. *Geophysical Research Letters*, 34:24206–24212.
- H. Bonnet, R. Abuter, A. Baker, W. Bornemann, A. Brown, R. Castillo, R. D. Conzelmann, R. Damster, R. Davies, B. Delabre, R. Donaldson, C. Dumas, F. Eisenhauer, E. Elswijk, E. Fedrigo, G. Finger, H. Gemperlein, R. Genzel, A. Gilbert, G. Gillet, A. Goldbrunner, M. Horrobin, R. Ter Horst, S. Huber, N. N. Hubin, C. Iserlohe, A. Kaufer, M. Kissler-Patig, J. Kragt, G. Kroes, M. D. Lehnert, W. Lieb, J. Liske, J.-L. Lizon, D. Lutz, A. Modigliani, G. J. Monnet, N. Nesvadba, J. Patig, J. Pragt, J. Reunanen, C. Röhrle, S. Rossi, R. Schmutzer, T. Schoenmaker, J. Schreiber, S. Stroebele, T. Szeifert, L. Tacconi, M. Tecza, N. A. Thatte, S. Tordo, P. van der Werf, and H. Weisz, 2004. First light of SINFONI at the VLT. *The Messenger*, 117:17–24.
- H. Bonnet, S. Ströbele, F. Biancat-Marchet, J. Brynnel, R. D. Conzelmann, B. Delabre, R. Donaldson, J. Farinato, E. Fedrigo, N. N. Hubin, M. E. Kasper, and M. Kissler-Patig, 2003. Implementation of MACAO for SINFONI at the VLT, in NGS and LGS modes. *SPIE*, 4839:329–343.

- R. Brunetto, P. Vernazza, S. Marchi, M. Birlan, M. Fulchignoni, V. Orofino, and G. Strazzulla, 2006. Modeling asteroid surfaces from observations and irradiation experiments: The case of 832 Karin. *Icarus*, 184:327–337.
- S. J. Bus and R. P. Binzel, 2002. Phase II of the Small Main-Belt Asteroid Spectroscopic Survey: The Observations. *Icarus*, 158:106–145.
- V. Carruba, T. A. Michtchenko, F. Roig, S. Ferraz-Mello, and D. Nesvorný, 2005. On the V-type asteroids outside the Vesta family. I. Interplay of non-linear secular resonances and the Yarkovsky effect: the cases of 956 Elisa and 809 Lundia. *Astronomy and Astrophysics*, 441:819–829.
- B. Carry, C. Dumas, M. Fulchignoni, W. J. Merline, J. Berthier, D. Hestroffer, T. Fusco, and P. Tamblyn, 2008. Near-Infrared Mapping and Physical Properties of the Dwarf-Planet Ceres. *Astronomy and Astrophysics*, 478(4): 235–244.
- C. R. Chapman, 2004. Space Weathering of Asteroid Surfaces. *Annual Review of Earth and Planetary Sciences*, 32:539–567.
- F. E. DeMeo, R. P. Binzel, S. M. Slivan, and S. J. Bus, 2009. An extension of the Bus asteroid taxonomy into the near-infrared. *Icarus*. doi:10.1016/j.icarus.2009.02.005.
- F. Eisenhauer, R. Abuter, K. Bickert, F. Biancat-Marchet, H. Bonnet, J. Brynneel, R. D. Conzelmann, B. Delabre, R. Donaldson, J. Farinato, E. Fedrigo, R. Genzel, N. N. Hubin, C. Iserlohe, M. E. Kasper, M. Kissler-Patig, G. J. Monnet, C. Roehrl, J. Schreiber, S. Stroebel, M. Tecza, N. A. Thatte, and H. Weisz, 2003. SINFONI - Integral field spectroscopy at 50 milli-arcsecond resolution with the ESO VLT. *SPIE*, 4841:1548–1561.
- M. A. Feigerberg and M. J. Drake, 1980. The meteorite-asteroid connection - The infrared spectra of eucrites, shergottites, and Vesta. *Science*, 209:805–807.
- M. A. Feigerberg, H. P. Larson, U. Fink, and H. A. Smith, 1980. Spectroscopic evidence for two achondrite parent bodies - Asteroids 349 Dembowska and 4 Vesta. *Geochimica et Cosmochimica Acta*, 44:513–524.
- M. J. Gaffey. The Asteroid (4) Vesta: Rotational Spectral Variations, Surface Material Heterogeneity, and Implications for the Origin of the Basaltic Achondrites. In *Lunar and Planetary Institute Conference Abstracts*, volume 14 of *Lunar and Planetary Institute Conference Abstracts*, pages 231–232, 1983.
- M. J. Gaffey, 1997. Surface Lithologic Heterogeneity of Asteroid 4 Vesta. *Icarus*, 127:130–157.
- M. J. Gaffey, E. A. Cloutis, M. S. Kelley, and K. L. Reed, 2002. Mineralogy of Asteroids. *Asteroids III*, pages 183–204.
- A. R. Hendrix, F. Vilas, and M. C. Festou, 2003. Vesta's UV lightcurve: hemispheric variation in brightness and spectral reversal. *Icarus*, 162:1–9.
- T. Hiroi, R. P. Binzel, J. M. Sunshine, C. M. Pieters, and H. Takeda, 1995. Grain sizes and mineral compositions of surface regoliths of Vesta-like asteroids. *Icarus*, 115:374–386.
- T. Hiroi and C. M. Pieters, 1998. Origin of vestoids suggested from the space weathering trend in the visible reflectance spectra of HED meteorites and lunar soils. *Antarctic Meteorite Research*, 11:163–170.
- K. Keil, 2002. Geological History of Asteroid 4 Vesta: The "Smallest Terrestrial Planet". *Asteroids III*, pages 573–584.
- H. P. Larson and U. Fink, 1975. Infrared spectral observations of Asteroid 4 Vesta. *Icarus*, 26:420–427.
- D. Lazzaro, T. Michtchenko, J. M. Carvano, R. P. Binzel, S. J. Bus, T. H. Burbine, T. Mothé-Diniz, M. Florczak, and C. A. Angeli, 2000. Discovery of a Basaltic Asteroid in the Outer Main Belt. *Science*, 288(5473):2033–2035.
- J.-Y. Li, L. A. McFadden, P. C. Thomas, M. J. Mutchler, J. W. Parker, E. F. Young, C. T. Russell, M. V. Sykes, and B. Schmidt, 2008. Photometric mapping of Vesta from HST observations. *ACM Meeting*. Poster 8288.
- S. Marchi, R. Brunetto, S. Magrin, M. Lazzarin, and D. Gandolfi, 2005a. Space weathering of near-Earth and main belt silicate-rich asteroids: observations and ion irradiation experiments. *Astronomy and Astrophysics*, 443:769–775.
- S. Marchi, M. Lazzarin, P. Paolicchi, and S. Magrin, 2005b. New V-type asteroids in near-Earth space. *Icarus*, 175:170–174.
- F. Marzari, A. Cellino, D. R. Davis, P. Farinella, V. Zappala, and V. Vanzani, 1996. Origin and evolution of the Vesta asteroid family. *Astronomy and Astrophysics*, 316:248–262.
- T. B. McCord, J. B. Adams, and T. V. Johnson, 1970. Asteroid Vesta: Spectral Reflectivity and Compositional Implications. *Science*, 168(3938):1445–1447.
- L. A. McFadden, T. B. McCord, and C. M. Pieters, 1977. Vesta - the first pyroxene band from new spectroscopic measurements. *Icarus*, 31(4):439–446.
- N. A. Moskovitz, R. Jedicke, E. Gaidos, M. Willman, D. Nesvorný, R. Fevig, and Ž. Ivezić, 2008. The distribution of basaltic asteroids in the Main Belt. *Icarus*, 198:77–90.
- D. Nesvorný, F. Roig, B. J. Gladman, D. Lazzaro, V. Carruba, and T. Mothé-Diniz, 2008. Fugitives from the Vesta family. *Icarus*, 193:85–95.
- C. M. Pieters, R. P. Binzel, D. Bogard, T. Hiroi, D. W. Mittlefehldt, L. E. Nyquist, A. S. Rivkin, and H. Takeda. Asteroid-meteorite links: The Vesta conundrum(s). In D. Lazzaro, S. Ferraz-Mello, and J. A. Fernández, editors, *Asteroids Comets Meteors Proceedings of the 229th Symposium of the International Astronomical Union*, pages 273–288. Cambridge University Press., 2006.
- C. M. Pieters, L. A. Taylor, S. K. Noble, L. P. Keller, B. Hapke, R. V. Morris, C. C. Allen, D. S. McKay, and S. Wentworth, 2000. Space weathering on airless bodies: Resolving a mystery with lunar samples. *Meteoritics and Planetary Science*, 35:1101–1107.
- N. C. Richmond and L. L. Hood, 2008. A preliminary global map of the vector lunar crustal magnetic field based on Lunar Prospector magnetometer data. *Journal of Geophysical Research*, 113:2010–2025.
- S. Sasaki, K. Nakamura, Y. Hamabe, E. Kurahashi, and T. Hiroi, 2001. Production of iron nanoparticles by laser irradiation in a simulation of lunar-like space weathering. *Nature*, 410:555–557.
- P. K. Seidelmann, B. A. Archinal, M. F. A'Hearn, A. Conrad, G. J. Consolmagno, D. Hestroffer, J. L. Hilton, G. A. Krasinsky, G. Neumann, J. Oberst, P. Stooke, E. F. Tedesco, D. J. Tholen, P. C. Thomas, and I. P. Williams, 2007. Report of the IAU/IAG Working Group on cartographic coordinates and rotational elements: 2006. *Celestial Mechanics and Dynamical Astronomy*, 98:155–180.
- D. I. Shestopalov and L. F. Golubeva, 2008. Why Vesta's Surface is Unweathered? *LPI Contributions*, 39:1116–1117.
- G. Strazzulla, E. Dotto, R. P. Binzel, R. Brunetto, M. A. Barucci, A. Blanco, and V. Orofino, 2005. Spectral alteration of the Meteorite Epinal (H5) induced by heavy ion irradiation: a simulation of space weathering effects on near-Earth asteroids. *Icarus*, 174:31–35.
- P. C. Thomas, R. P. Binzel, M. J. Gaffey, A. D. Storrs, E. N. Wells, and B. H. Zellner, 1997a. Impact excavation on asteroid 4 Vesta: Hubble Space Telescope results. *Science*, 277:1492–1495.
- P. C. Thomas, R. P. Binzel, M. J. Gaffey, B. H. Zellner, A. D. Storrs, and E. N. Wells, 1997b. Vesta: Spin Pole, Size, and Shape from HST Images. *Icarus*, 128:88–94.
- P. Vernazza, R. P. Binzel, A. Rossi, M. Fulchignoni, and M. Birlan, 2009. Solar wind as the origin of rapid reddening of asteroid surfaces. *Nature*, 458: 993–995.
- P. Vernazza, R. Brunetto, G. Strazzulla, M. Fulchignoni, P. Rochette, N. Meyer-Vernet, and I. Zouganelis, 2006. Asteroid colors: a novel tool for magnetic field detection? The case of Vesta. *Astronomy and Astrophysics*, 451:43–46.
- P. Vernazza, T. Mothé-Diniz, M. A. Barucci, M. Birlan, J. M. Carvano, G. Strazzulla, M. Fulchignoni, and A. Migliorini, 2005. Analysis of near-IR spectra of 1 Ceres and 4 Vesta, targets of the Dawn mission. *Astronomy and Astrophysics*, 436:1113–1121.
- J. G. Williams, 1989. Asteroid family identifications and proper elements. *Asteroids II*, pages 1034–1072.
- S. Xu, R. P. Binzel, T. H. Burbine, and S. J. Bus, 1995. Small Main-belt Asteroid Spectroscopic Survey: Initial results. *Icarus*, 115:1–35.
- V. Zappala, A. Cellino, P. Farinella, and Z. Knežević, 1990. Asteroid families. I - Identification by hierarchical clustering and reliability assessment. *Astronomical Journal*, 100:2030–2046.
- B. H. Zellner, R. Albrecht, R. P. Binzel, M. J. Gaffey, P. C. Thomas, A. D. Storrs, and E. N. Wells, 1997. Hubble Space Telescope Images of Asteroid 4 Vesta in 1994. *Icarus*, 128:83–87.
- N. E. B. Zellner, S. Gibbard, I. de Pater, F. Marchis, and M. J. Gaffey, 2005. Near-IR imaging of Asteroid 4 Vesta. *Icarus*, 177:190–195.